Atmospheric Environment 46 (2012) 71–80

Contents lists available at SciVerse ScienceDirect

Atmospheric Environment

journal homepage: www.elsevier.com/locate/atmosenv

A CFD modeling study of the impacts of NO_x and VOC emissions on reactive pollutant dispersion in and above a street canyon

Kyung-Hwan Kwak, Jong-Jin Baik*

School of Earth and Environmental Sciences, Seoul National University, Seoul 151-742, Republic of Korea

ARTICLE INFO

Article history:
Received 16 June 2011
Received in revised form
5 October 2011
Accepted 12 October 2011

Keywords:
Street canyon
CFD model
CBM-IV
VOC-to-NO_x emission ratio
Dispersion type
O_3 sensitivity

ABSTRACT

A computational fluid dynamics (CFD) model that includes the carbon bond mechanism IV (CBM-IV) is developed and used to investigate reactive pollutant dispersion in and above a street canyon with an aspect ratio of 1. Fourteen emission scenarios of NO_x and volatile organic compounds (VOCs) are considered. Dispersion types are classified into NO-type, NO_2-type, and O_3-type dispersion that exhibit concentration maxima at the street bottom, near the center of the street canyon, and above the street canyon, respectively. For the base emission scenario, the number of reactive species is 9 in the NO-type dispersion, 10 in the NO_2-type dispersion, and 15 in the O_3-type dispersion. As the NO_x emission level decreases or the VOC emission level increases, some species in the O_3-type dispersion are shifted to the NO_2-type dispersion. The VOC-to-NO_x emission ratio is found to be an important factor in determining the transition of dispersion type. In this transition process, OH plays a key role through a radical chain including HO_2, RO, and RO_2. Because of their high OH reactivities, XYL (xylene) and OLE (olefin carbon bond) among VOCs are largely responsible for the transition of dispersion type. The O_3 sensitivity is examined by reducing NO_x or VOC emission level by a half. Because the NO titration of O_3 is more pronounced than the NO_2 photolysis and the radical chain process in the street canyon, the O_3 concentration therein is negatively correlated with the NO_x emission level and weakly correlated with the VOC emission level. As a result, the street canyon is a negatively NO_x-sensitive regime.

1. Introduction

Air pollution in cities is a serious environmental problem. Not only primary pollutants such as NO_x ($NO + NO_2$) and volatile organic compounds (VOCs) from mobile sources but also secondary pollutants such as ozone (O_3) cause public health problems for urban dwellers. Many observational and numerical modeling studies have shown that the O_3 concentration in urban areas is generally more sensitive to VOC emission than to NO_x emission (Peng et al., 2006; Lei et al., 2007; Martins and Andrade, 2008). However, the O_3 sensitivity to its precursors is diverse depending on the source characteristics. Near the center of a megacity where the VOC-to-NO_x emission ratio is relatively low owing to an abundance of mobile sources, the O_3 concentration tends to decrease significantly as NO_x emission increases (Jenkin and Clemitshaw, 2000; Zavala et al., 2009). This indicates that the chemical behaviors of pollutants in proximity to their sources can differ from the behaviors generally found for broad-scale urban areas.

There are a few numerical modeling studies that consider several chemical reactions to investigate the dispersion of reactive pollutants near a vehicular exhaust tailpipe (Chan et al., 2001) and in street canyons (Baker et al., 2004; Baik et al., 2007; Grawe et al., 2007; Kang et al., 2008). An investigation of NO_x dispersion using the Monte Carlo method showed that the oxidation reduction of NO and thus the formation and accumulation of NO_2 in a vehicular exhaust plume are important at the initial dispersion process near a tailpipe (Chan et al., 2001). Baker et al. (2004) examined the dispersion of NO, NO_2, and O_3 in a street canyon using a large-eddy simulation (LES) model that includes simple photochemistry among the reactive pollutants. Baik et al. (2007) developed a Reynolds-averaged Navier–Stokes equations (RANS) model coupled with the simple photochemistry of $NO–NO_2–O_3$ and used this model to examine the temperature-dependent dispersion of the reactive pollutants in a street canyon. Baker et al. (2004) and Baik et al. (2007) found that a chemically unstable region exists near the roof level. The dispersion of reactive pollutants in a street canyon is known to be affected by shadowing (Grawe et al., 2007) and surface heating (Kang et al., 2008).

In addition to the simple photochemistry, some VOCs and their reactions have recently been included in numerical models used to

* Corresponding author. Tel.: +82 2 880 6990; fax: +82 2 883 4972.
E-mail address: jjbaik@snu.ac.kr (J.-J. Baik).

1352-2310/$ – see front matter © 2011 Elsevier Ltd. All rights reserved.
doi:10.1016/j.atmosenv.2011.10.024

calculate the concentrations of various reactive pollutants in street canyons (Liu and Leung, 2008; Garmory et al., 2009). Liu and Leung (2008) examined O_3 formation in street canyons using a chemistry box model. Using the field Monte Carlo method, Garmory et al. (2009) showed that some radical species in the carbon bond mechanism IV (CBM-IV) deviate significantly from the chemical equilibrium at the roof-top level.

Focusing on street canyons, the dispersion of various reactive pollutants is still not well understood. The CBM-IV that includes both NO_x and VOC chemistry is useful for studying not only mesoscale regional chemistry but also microscale urban chemistry (Kim et al., 2008; Garmory et al., 2009). We have developed a computational fluid dynamics (CFD) model coupled with the CBM-IV to study urban flow and reactive pollutant dispersion. In this paper, the CFD model developed is introduced and the dispersion of reactive pollutants in and above a street canyon is examined. Furthermore, the O_3 sensitivity to the NO_x and VOC emission levels is examined. This study is an attempt to analyze the dispersion of tens of reactive pollutants in and above a street canyon using a CFD model.

2. CFD model, validation, and experimental setup

2.1. Chemical mechanism

The CBM-IV adopted for this study has 36 reactive species and 93 reactions (Gery et al., 1989). The reactive species in the CBM-IV are listed in Table 1. VOCs are lumped in terms of carbon bond structures. PAR is a one-carbon surrogate for alkanes with a carbon single bond. OLE is a two-carbon surrogate for alkenes with a carbon double bond. ALD_2 is a two-carbon carbonyl surrogate for acetaldehydes or higher aldehydes. TOL and XYL are representations for lumped species with mono-alkyl-benzene structures (seven-carbon species) and di- or tri-alkyl-benzene structures (eight- or nine-carbon species), respectively. In contrast to the lumped species above, FORM and ETH are representations for single species that are formaldehyde and ethene, respectively. Simple isoprene (ISOP) chemistry is included (Carter, 1996).

Table 1
Reactive species in the CBM-IV.

Representation	Species name
Explicit method (13 species)	
NO	Nitric oxide
NO_2	Nitrogen dioxide
NO_3	Nitrate radical
N_2O_5	Dinitrogen pentoxide
HONO	Nitrous acid
PNA	Peroxynitric acid
O^1D	Oxygen atom $O^1(D)$
O	Oxygen atom $O^3(P)$
OH	Hydroxyl radical
O_3	Ozone
HO_2	Hydroperoxy radical
C_2O_3	Peroxyacyl radical
PAN	Peroxyacyl nitrate
EBI method (23 species)	
HNO_3	Nitric acid
H_2O_2	Hydrogen peroxide
CO	Carbon monoxide
FORM	Formaldehyde
ALD_2	High molecular weight aldehydes
PAR	Paraffin carbon bond
ROR	Secondary organic oxy radical
NTR	Organic nitrate
OLE	Olefin carbon bond
ETH	Ethene
TOL	Toluene
CRES	Cresol and higher molecular weight phenols
TO_2	Toluene-hydroxyl radical adduct
CRO	Methylphenoxy radical
OPEN	High molecular weight aromatic oxidation ring fragment
XYL	Xylene
MGLY	Methylglyoxal
ISOP	Isoprene
ISPD	Isoprene product
XO_2	NO-to-NO_2 operation
XO_2N	NO-to-nitrate operation
SO_2	Sulfur dioxide
SULF	Sulfuric acid (gaseous)

2.2. CFD model

The CFD model used to couple the CBM-IV is a RANS model with the renormalization group (RNG) $k-\varepsilon$ turbulence closure scheme (Kim and Baik, 2004; Baik et al., 2007). The governing equations are the momentum equation, the mass continuity equation, and the equations of turbulent kinetic energy and its dissipation rate. The transport equation of a reactive species is given as

$$\frac{\partial C_i}{\partial t} + U_j\frac{\partial C_i}{\partial x_j} = D\frac{\partial^2 C_i}{\partial x_j \partial x_j} + \frac{\partial}{\partial x_j}\left(K_c\frac{\partial C_i}{\partial x_j}\right) + \left[\frac{\partial C_i}{\partial t}\right]_{\text{chem}}. \quad (1)$$

Here, C_i is the concentration of the ith reactive species, U_j the jth mean velocity component, D the molecular diffusivity of the species, and K_c the eddy diffusivity of the species. The last term denotes the net chemical production rate of the species calculated by the CBM-IV. The reaction coefficients in the CBM-IV are calculated at the atmospheric pressure and at the air temperature of 298 K, and the photolysis rate coefficients of NO_2, NO_3, HONO, O_3, H_2O_2, FORM, ALD_2, OPEN, MGLY, and ISPD are obtained from Jacobson (2005). The Eulerian backward iteration (EBI) method (Hertel et al., 1993) is used as a chemical solver to integrate the stiff system of photochemical reactions. Of the 36 reactive species in the CBM-IV, 23 are regarded as the species whose concentrations are calculated using the EBI method. The concentrations of the other 13 species are explicitly calculated (Table 1).

2.3. Validation

The coupled CFD model is validated for NO_2 and NO_x concentrations against the field experiment data obtained during the Texas Roadway Study on 13 July 2007 (Zhu et al., 2009; Clements et al., 2009). The target road has two track lines, a width of 8.5 m, and a traffic volume of 1038 vehicles h^{-1}. During the measurement period, the wind direction is nearly perpendicular to the road. In this validation simulation, the background concentrations of NO_2, NO_x, O_3, HO_2, RO_2, HCHO, and CH_3CHO, the roadside concentrations of NO_2 and NO_x (source strength), the road temperature, and other meteorological parameters summarized in Wang et al. (2011) are used and the thermodynamic energy equation is included. Following Wang et al. (2011), 4 measurement points at the distances of 14, 62, 109, and 157 m from the road are considered for this validation.

Fig. 1 shows the simulated and measured NO_2 and NO_x concentrations as a function of distance. The simulated NO_2 concentrations are slightly overestimated. The difference between the simulated and measured NO_2 concentrations decreases with increasing distance from the road. This difference is 1.4 ppb at the nearest point and 0.17 ppb at the farthest point. In contrast, the simulated NO_x concentrations match the measured values very well. From Fig. 1, it is inferred that the NO-to-NO_2 conversion in the simulation is greater than the actual conversion especially near the road. To some extent, this might be due to the uncertainties in the initial NO_2-to-NO_x ratio and the NO_2 photolysis rate coefficient.

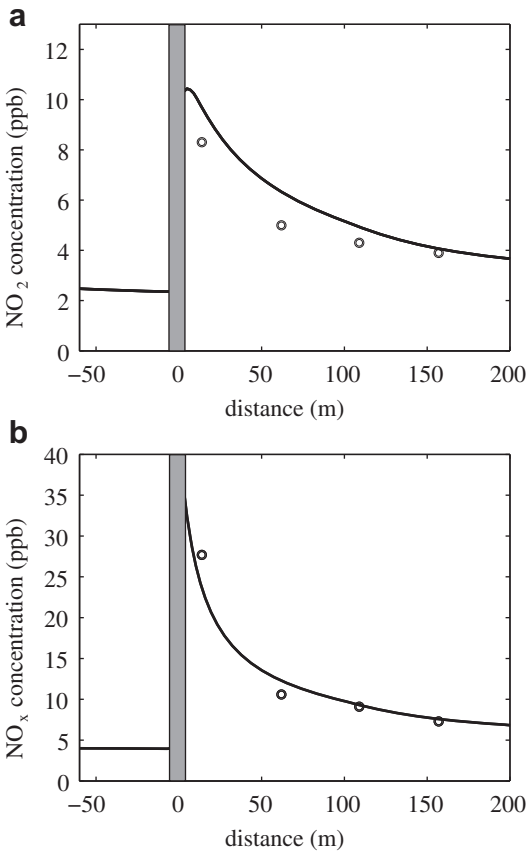

Fig. 1. (a) NO_2 and (b) NO_x concentrations with distance in the simulation (line) and measurement (circle). The road is shaded.

Overall, the CFD model coupled with the CBM-IV successfully simulates the NO_2-to-NO_x ratio that is an important indicator for urban atmospheric chemistry. The NO_2-to-NO_x ratio at a distance of 62 m from the road is 0.52 in the simulation and 0.47 in the measurement.

2.4. Experimental setup

Fig. 2 illustrates a two-dimensional domain and an idealized street canyon. Both the building height (H) and the street canyon width (W) are 20 m, giving a canyon aspect ratio (H/W) of 1. The domain size is 40 m in the x-direction and 60.1 m in the z-direction. The grid interval is 0.5 m in the x-direction. The grid interval in the z-direction is 0.5 m up to $z = 32$ m and then gradually increases with an expansion ratio of 1.1. The ambient wind blows in the x-direction. The boundary conditions for the velocity components, turbulent kinetic energy, and its dissipation rate follow Baik et al. (2007). For example, the ambient wind speed at the roof level of the inflow boundary is 3.9 m s^{-1}. The isothermal condition is applied, assuming the air temperature of 298 K. For concentrations, the cyclic boundary condition in the x-direction is applied at the inflow and outflow boundaries and the zero-gradient boundary condition is applied at the upper boundary. An area source of 9 emission species (NO, NO_2, FORM, ALD_2, PAR, OLE, ETH, TOL, and XYL) is located at the lowest model level ($z/H = 0.0125$; hereafter referred to as the street bottom) in the street canyon. The CFD model is integrated for 90 min with a time step of 0.1 s.

The initial concentrations of all reactive species are calculated using a chemistry box model composed of the same chemical mechanism and chemical solver. Concentrations calculated by a 1-h simulation of the chemistry box model reach an approximately quasi-steady state, while the concentrations of 9 emission species and O_3 are constrained at 10 ppb (NO), 30 ppb (NO_2), 30 ppb (O_3), and 40 ppb (7 VOCs in total). The relative portions of the 7 VOC concentrations among the emission species in volume are 56.3% for PAR, 12.4% for TOL, 11.9% for XYL, 9.5% for ETH, 6.7% for OLE, 2.1% for ALD_2, and 1.1% for FORM (Smylie et al., 1991; Bossioli et al., 2002). For the first 30 min of time integration, the concentrations of all reactive species are calculated without emission and chemical production or loss. After $t = 30$ min, the concentrations are calculated by considering advection, diffusion, emission, and chemical processes simultaneously at every time step. All results are analyzed at $t = 90$ min when the concentrations of reactive species are in an approximately pseudo-steady state in the street canyon.

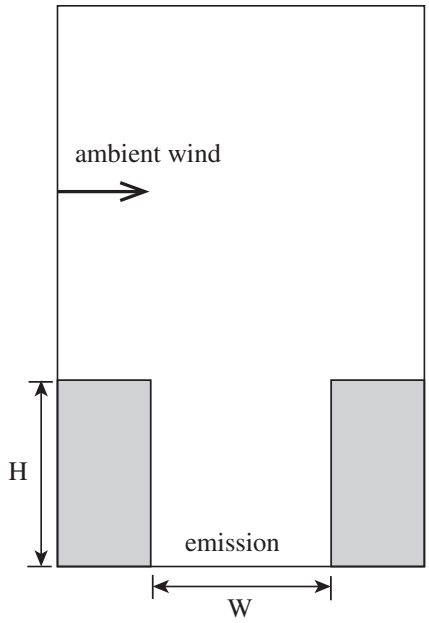

Fig. 2. Illustration of computational domain and buildings. H is the building height and W is the street canyon width.

Table 2 shows 14 emission scenarios of NO_x and VOCs with the same relative portions of the 7 VOC concentrations in the chemistry box model simulation. For analyzing the dispersion of reactive species in an approximately pseudo-steady state, concentrations of 9 emission species at the street bottom are specified as emission levels. Here, the NO_x and VOC concentrations of 300 ppb are designated as emission levels of 1.0 NO_x and 1.0 VOC, respectively.

Table 2
Emission scenarios for NO_x and 7 VOCs.

No.	NO_x (ppb)	7 VOCs (ppb)	VOC/NO_x	O_3 sensitivity
S1	150	300	2.00	O
S2	225	300	1.33	X
S3 (base)	300 (1.0 NO_x)	300 (1.0 VOC)	1.00	O
S4	375	300	0.80	X
S5	450	300	0.67	X
S6	150	600	4.00	X
S7	225	600	2.67	X
S8	300	600	2.00	X
S9	375	600	1.60	X
S10	450	600	1.33	X
S11	300	150	0.50	O
S12	300	450	1.50	X
S13	300	750	2.50	X
S14	300	900	3.00	X

The 14 emission scenarios cover the ratio of VOC emission to NO_x emission (the VOC-to-NO_x emission ratio) ranging from 0.5 (1.0 NO_x and 0.5 VOC) to 4 (0.5 NO_x and 2.0 VOC). Three emission scenarios in the last column of Table 2 are used to examine the O_3 sensitivity (subsection 3.3). In this study, two species (SO_2 and SULF) out of the 36 species in the CBM-IV are excluded for neglecting sulfur chemistry.

3. Results and discussion

3.1. Dispersion type

The dispersion of NO, NO_2, and O_3 in street canyons using the simple photochemistry among them was numerically investigated by Baker et al. (2004), Baik et al. (2007), and Garmory et al. (2009). Garmory et al. (2009) examined the dispersion using the simple photochemistry and also the CBM-IV and indicated that NO, NO_2, and O_3 concentrations calculated using the CBM-IV are similar to those calculated using the simple photochemistry within approximately 1 ppb for the same experimental setting. However, they did not consider VOC emission and its impacts on O_3 concentration in the simulations. Here, we first examine the dispersion of NO, NO_2, and O_3 with the complexity of VOC chemistry. Then, we examine the dispersion of other reactive species and compare it to the dispersion of NO, NO_2, and O_3.

Fig. 3 shows the streamline field and the NO, NO_2, and O_3 concentration fields in and above the street canyon for the emission scenario of 1.0 NO_x and 1.0 VOC (S3; base scenario). A primary vortex is formed in the street canyon. Because the less-polluted ambient air flows into the street canyon near the downwind building wall, the NO concentration is lower near the downwind building wall than near the upwind building wall. The NO_2 concentration is broadly high over 55 ppb around the center of the street canyon. Because the NO_2 concentration above the street canyon is also comparably high, there is no significant impact of inflow on the concentration near the downwind building wall. The O_3 concentration below 30 ppb in the street canyon is primarily the result of the $NO + O_3 \rightarrow NO_2$ reaction (NO titration of O_3) that is a major sink of O_3. Around the center of the street canyon, the low NO and high NO_2 concentrations coincide with the low O_3 concentration. NO, NO_2, and O_3 do not reach a photo-stationary state among them because chemical O_3 loss due to the NO titration is not exactly balanced by chemical O_3 production due to the NO_2 photolysis. In the street canyon, the NO titration of O_3 that is more pronounced than the NO_2 photolysis causes the net chemical O_3 loss. The chemical O_3 loss is substantially compensated by the inflow of O_3 from the ambient air. Above the street canyon, the NO_2 photolysis that is more pronounced than the NO titration of O_3 causes the net chemical O_3 production. In addition to the differences in experimental setting, this chemical imbalance explains why the dispersion pattern of NO_2 in the street canyon that we found differs from the result of Baker et al. (2004) using the simple photochemistry that assumes a photo-stationary state for NO, NO_2, and O_3.

Dispersion types of other reactive species are classified into the NO-type, NO_2-type, and O_3-type dispersion. The NO-type and NO_2-type dispersion are identified when the concentration is maximized at the street bottom and near the center of the street canyon, respectively. The species in these two dispersion types show higher concentrations in the street canyon than above it. The O_3-type dispersion is identified when the concentration is higher above the street canyon than in it.

Fig. 4 shows the vertical profiles of the street canyon width-averaged concentrations. The average is taken over the street canyon width from $x/H = -0.5$ to 0.5. Each species concentration is normalized by the corresponding concentration at the street bottom. Based on their vertical profiles, 9 species (NO, HONO, ALD_2, PAR, ROR, OLE, ETH, TOL, and XYL) are classified into the NO-type dispersion (Fig. 4a). Out of the 9 species, 7 species are emission species for which their concentrations are specified at the street

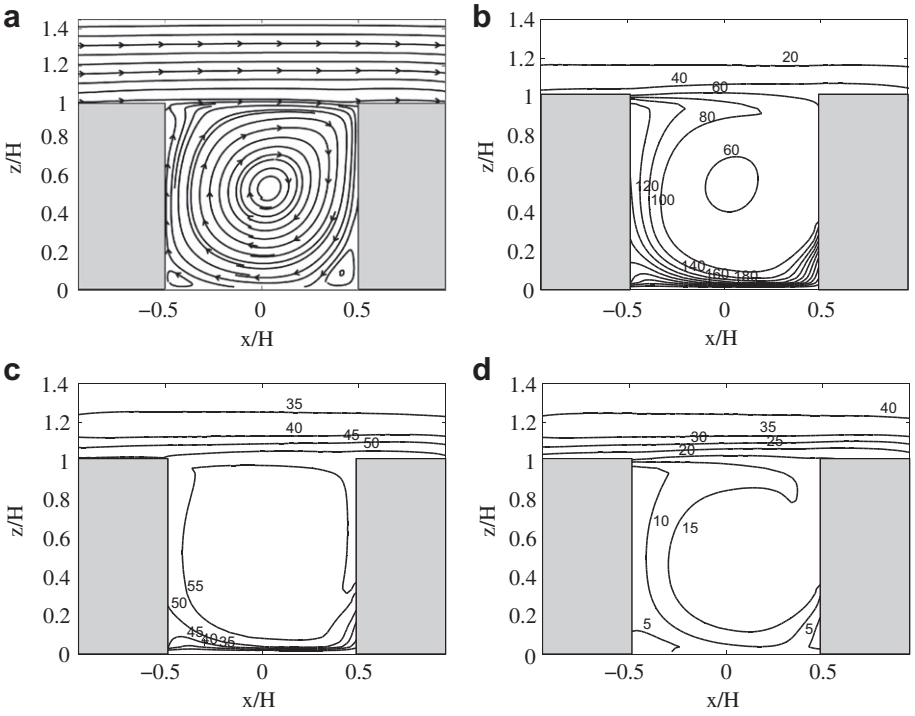

Fig. 3. (a) Streamline field and (b) NO, (c) NO_2, and (d) O_3 concentration fields in and above the street canyon for the emission scenario of 1.0 NO_x and 1.0 VOC.

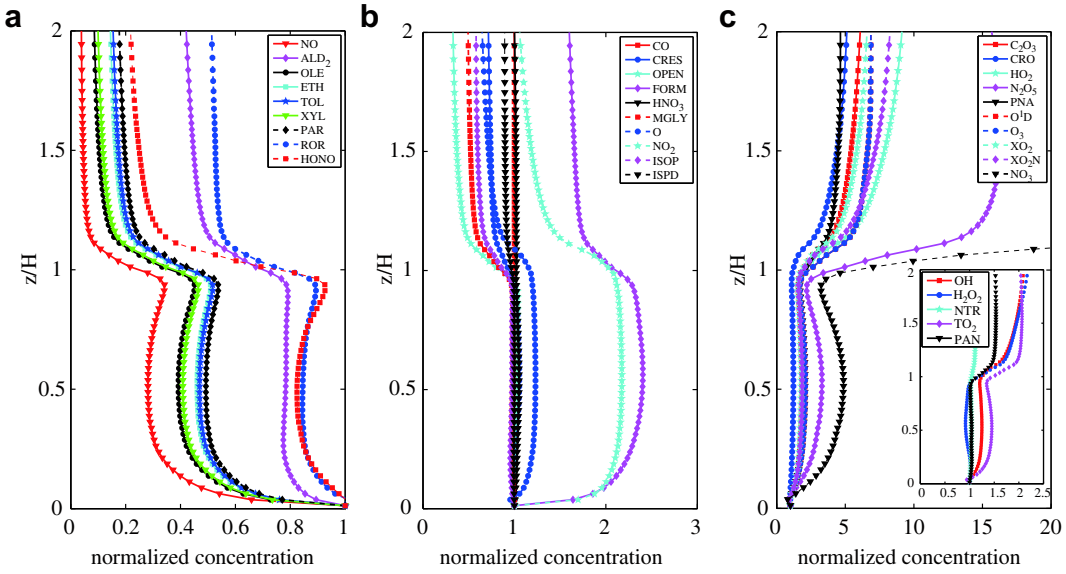

Fig. 4. Vertical profiles of the street canyon width-averaged concentrations of species in (a) NO-type dispersion, (b) NO_2-type dispersion, and (c) O_3-type dispersion for the emission scenario of 1.0 NO_x and 1.0 VOC. Each species concentration is normalized by that at the street bottom.

bottom. HONO and ROR are not emission species but can be directly produced by chemical reactions related to emission species. Ten species (NO_2, O, HNO_3, CO, FORM, CRES, OPEN, MGLY, ISOP, and ISPD) are classified into the NO_2-type dispersion (Fig. 4b). Their concentration maxima appear near $z/H = 0.5$. NO_2 and FORM are emission species but are effectively produced in the street canyon by the NO titration of O_3 and by the oxidation of VOCs, respectively. CO concentration (approximately 1 ppm) is relatively high compared to the concentrations of the other species. Chemical processes, therefore, barely affect the CO concentration in and above the street canyon and the difference in CO concentration between in and above the street canyon is insignificant. Fifteen species (NO_3, N_2O_5, PNA, O^1D, OH, O_3, HO_2, C_2O_3, PAN, H_2O_2, NTR, TO_2, CRO, XO_2, and XO_2N) are classified into the O_3-type dispersion (Fig. 4c). In this base scenario, all radical species except for O (NO_2-type) and ROR (NO-type) show the O_3-type dispersion. Species in the O_3-type dispersion experience large changes in normalized concentration with height as crossing the roof level. Because the street canyon is polluted with emission species, the chemical losses of highly reactive species are more promoted by their reactions with emission species in the street canyon than above it. Therefore, the rapid losses of highly reactive species lead to low concentrations in the street canyon compared to concentrations above the street canyon.

The dispersion type is not an inherent feature of a reactive species. The dispersion type may change in response to the emission level of NO_x or VOC. This is systematically analyzed for the emission scenarios of 0.5–1.5 NO_x with 1.0 VOC (S1–S5) and the emission scenarios of 0.5–3.0 VOC with 1.0 NO_x (S3, S8, S11–S14). While the NO-type dispersion is found to be invariable, transitions in dispersion type between the NO_2-type and the O_3-type dispersion are found to occur. The dispersion of HNO_3 is shifted from the NO_2-type dispersion (S3) to the O_3-type dispersion (S5, S11). In contrast, the dispersion of PNA, PAN, NTR, and TO_2 are shifted from the O_3-type dispersion (S3) to the NO_2-type dispersion (S1, S8, S12, S13, S14).

Fig. 5 shows the vertical profiles of the street canyon width-averaged PNA, PAN, NTR, and TO_2 concentrations for the 3 emission scenarios of 0.5, 1.0, and 1.5 NO_x with 1.0 VOC (S1, S3, S5). As the NO_x emission level decreases, the concentrations in the street canyon increase more markedly than those above it. This change leads to a transition from the O_3-type dispersion (S3, S5) to the NO_2-type dispersion (S1). Fig. 6 shows the vertical profiles of the street canyon width-averaged PNA, PAN, NTR, and TO_2 concentrations for the 3 emission scenarios of 1.0, 2.0, and 3.0 VOC with 1.0 NO_x (S3, S8, S14). As the VOC emission level increases, it is also clear that the concentrations in the street canyon increase more markedly than those above it. This change leads to a transition from the O_3-type dispersion (S3) to the NO_2-type dispersion (S8, S14). In addition to the 4 species, all species in the O_3-type dispersion except for two species (O_3 and O^1D) are apparently shifted to the NO_2-type dispersion for these emission scenarios (not shown). O_3 and O^1D remain invariable in dispersion type in response to the changes in the emission scenarios.

In summary, species in the NO_2-type and O_3-type dispersion generally tend to be classified into the NO_2-type dispersion as the NO_x emission level decreases or the VOC emission level increases. When both NO_x and VOC emission levels change, the effect of decreasing NO_x emission level on concentrations is mostly cancelled out by the effect of decreasing VOC emission level. For example, a typical reactive species would show almost the same vertical concentration profiles for the emission scenario of 1.0 NO_x and 2.0 VOC (S8) and for the emission scenario of 0.5 NO_x and 1.0 VOC (S1). Note that the VOC-to-NO_x emission ratio is equally 2 for these two emission scenarios. Hence, an important factor in determining the dispersion type of any species is the VOC-to-NO_x emission ratio rather than the separate emission level of NO_x or VOC. In the next subsection, we will discuss why the dispersion type depends on the VOC-to-NO_x emission ratio and will identify a key player that leads to the transitions between the dispersion types.

3.2. OH reactivity

The hydroxyl radical (OH) acts as a detergent in the troposphere. In the urban air, many pollutants such as VOCs and CO react easily with OH, thus initiating subsequent reactions (Sillman, 1999). Jenkin and Clemitshaw (2000) introduced a radical chain to describe the role of radical species such as OH, HO_2, RO, and RO_2 (Fig. 7). Here, R represents an alkyl-substituted group. In this radical

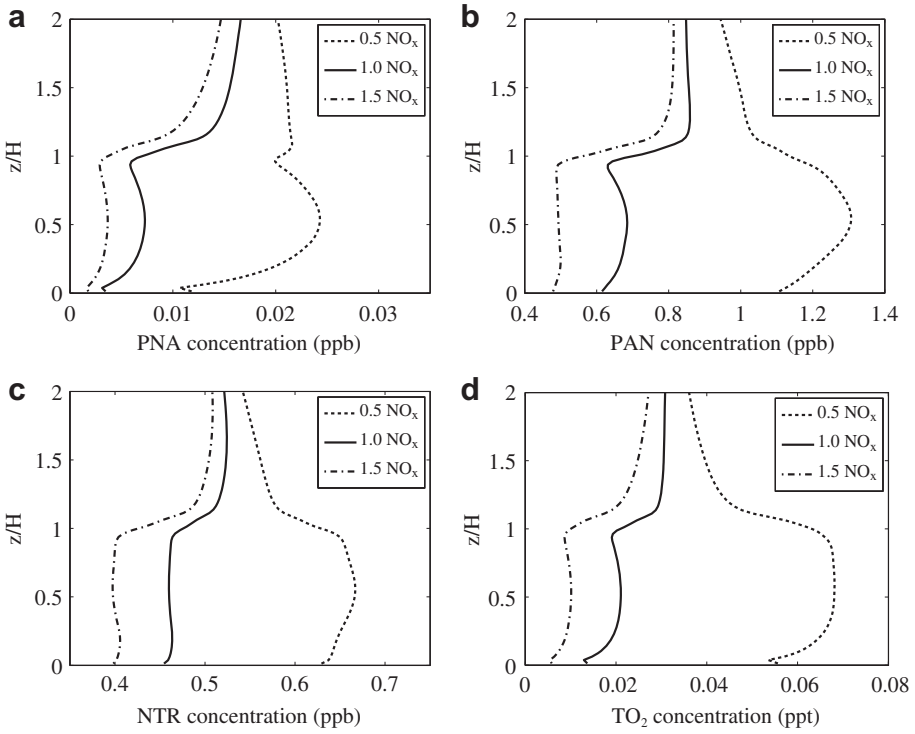

Fig. 5. Vertical profiles of the street canyon width-averaged concentrations of (a) PNA, (b) PAN, (c) NTR, and (d) TO_2 for the emission scenarios of 0.5, 1.0, and 1.5 NO_x with 1.0 VOC.

chain, the OH + NO_2 reaction contributes to the termination of the production of radical species, whereas the OH + RH reaction contributes to the propagation of the production of radical species. Therefore, the OH concentration controls the concentrations of other radical species through the OH + NO_2 reaction and the OH + RH reaction.

Fig. 8 shows the street canyon-averaged OH concentrations as a function of the NO_x (S1–S10) and VOC (S3, S8, S11–S14) emission

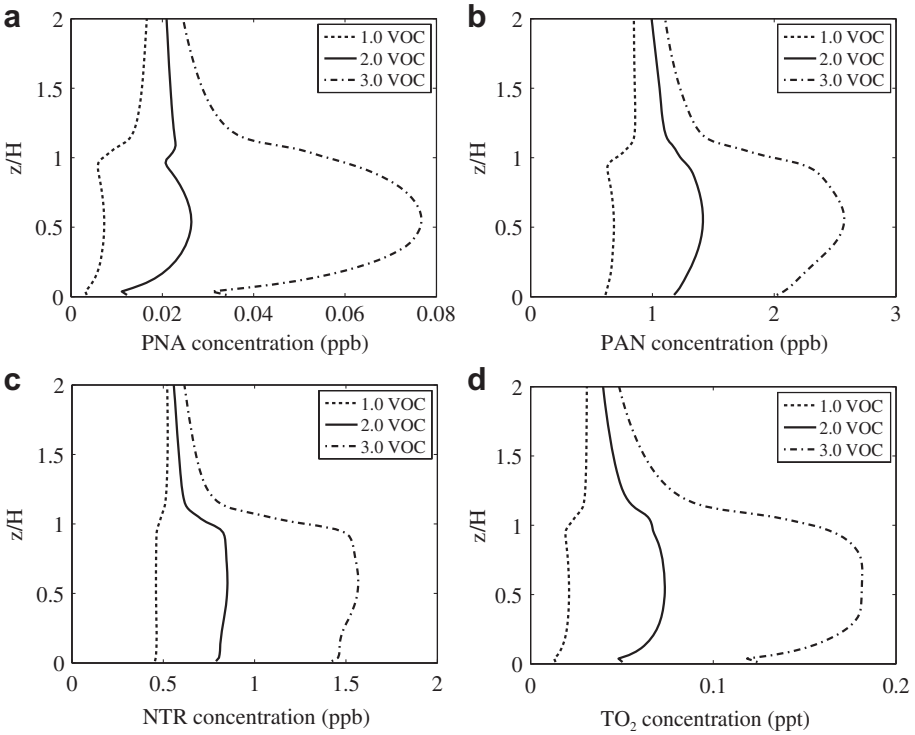

Fig. 6. Same as Fig. 5 but for the emission scenarios of 1.0, 2.0, and 3.0 VOC with 1.0 NO_x.

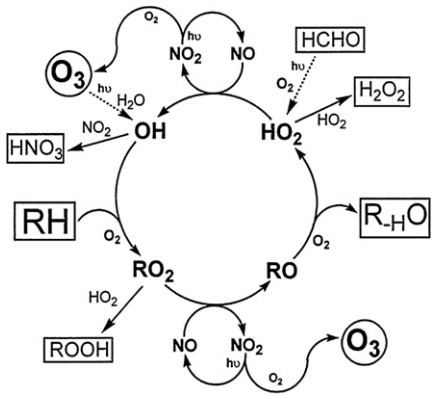

Fig. 7. Schematic representation of the radical chain propagation process (Jenkin and Clemitshaw, 2000).

levels. The street canyon average is taken from $x/H = -0.5$ to 0.5 and from $z/H = 0$ to 1. The OH concentration obviously decreases with increasing NO_x emission level from 0.5 to 1.5. However, the OH concentration almost linearly increases with increasing VOC emission level from 0.5 to 3.0. This dependence of the OH concentration on the NO_x and VOC emission levels, which is consistent with the dependence shown in the diagram of Sillman (1999) for the polluted urban air, can be explained by the radical chain shown in Fig. 7. An increase in the NO_x emission level enhances the role of the OH + NO_2 reaction to suppress the propagation of the radical chain, thus decreasing OH concentration. On the other hand, an increase in the VOC emission level enhances the role of the OH + RH reaction to promote the propagation of the radical chain, thus increasing OH concentration. In the propagation of the radical chain, decreasing (increasing) OH concentration reduces (raises) the concentrations of other radical species such as HO_2, RO, and RO_2.

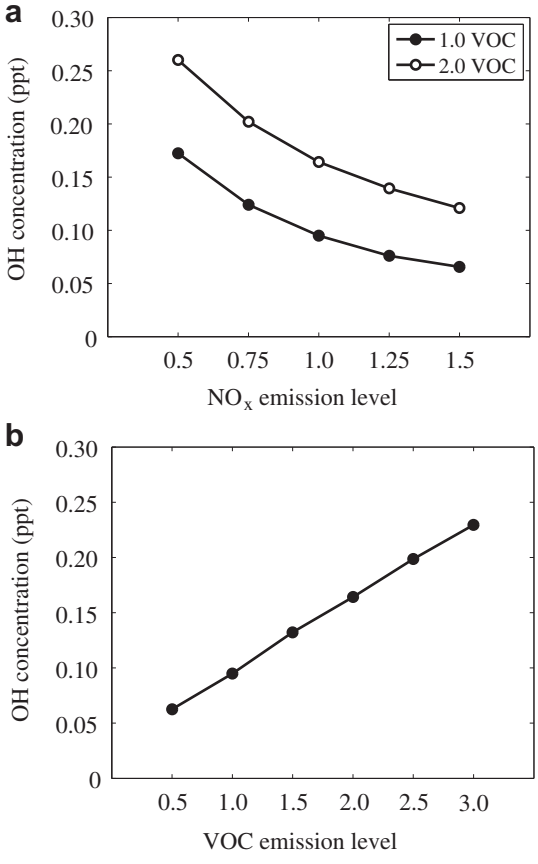

Fig. 8. Street canyon-averaged OH concentrations for the emission scenarios of (a) from 0.5 to 1.5 NO_x with 1.0 and 2.0 VOC and (b) from 0.5 to 3.0 VOC with 1.0 NO_x.

Fig. 9 shows the vertical profiles of the street canyon width-averaged concentrations of OH, HO_2, C_2O_3 and CRO for the emission scenarios of 0.5, 1.0, and 1.5 NO_x with 1.0 VOC (S1, S3, S5). Fig. 10 is the same as Fig. 9 but for the emission scenarios of 1.0, 2.0, and 3.0 VOC with 1.0 NO_x (S3, S8, S14). Figs. 9 and 10 verify what we discussed above, showing that the concentrations of HO_2, C_2O_3, and CRO are proportional to the OH concentration, which in turn depends on the NO_x and VOC emission levels. Here, C_2O_3 and CRO are examples of RO_2 and RO, respectively. Note that the concentrations of OH, HO_2, C_2O_3, and CRO decrease with increasing NO_x emission level (Fig. 9) but increase with increasing VOC emission level (Fig. 10). Therefore, the VOC-to-NO_x emission ratio controls the propagation of the radical chain through the OH + NO_2 reaction and the OH + RH reaction in opposite ways and hence it changes the concentrations of radical species and also their products. The changes in concentration are more apparent in the street canyon than above it because of the source location of NO_x and VOC. For this reason, the transitions between dispersion types occur depending on the VOC-to-NO_x emission ratio.

The reactivity of VOC, compared to the total amount of VOC, suitably represents an actual impact of VOC (Sillman, 1999). Understanding the relative reactivity of VOC is essential for measuring its actual effect on the initiation, propagation, and termination of relevant reactions. The OH reactivity (R_i), the reactivity of the ith VOC to OH, is calculated using

$$R_i = k_{OH+VOC_i}[VOC_i]. \quad (2)$$

Here, k_{OH+VOC_i} is the reaction coefficient between OH and the ith VOC and $[VOC_i]$ is the concentration of the ith VOC.

Fig. 11 shows the pie charts of the street canyon-averaged VOC concentrations and OH reactivities for the emission scenario of 1.0 NO_x and 1.0 VOC (S3). Each relative portion of the VOC concentrations is similar to the corresponding relative portion of the VOC emissions (Fig. 11a). However, each relative portion of the OH reactivities deviates significantly from the corresponding relative portion of the VOC emissions (Fig. 11b). Although PAR (54.7%) is the largest in relative portion of the concentrations, its rank in OH reactivity is sixth because of the small reaction coefficient of the OH + PAR reaction. XYL (33.4%) followed by OLE (21.3%), instead, is the largest in relative portion of the OH reactivities, indicating that XYL and OLE are responsible for more than a half of the total contribution to the OH + RH reaction in the street canyon. This rank in OH reactivity is consistent with the observation of Doraiswamy et al. (2009). They explained that the OH reactivities of ISOP, XYL, and OLE among the VOCs in the CBM-IV are higher than those of other VOCs at an urban site because the VOCs in the aromatic and olefin groups are highly reactive.

3.3. O_3 sensitivity

The O_3 concentration is sensitive to NO_x and VOC emission levels in different ways. Sillman (1999) reviewed two contrasting O_3-precursor relationships, the NO_x-sensitive and the VOC-sensitive chemical regimes. The NO_x-sensitive regime refers to situations in which a percent reduction in NO_x results in a significantly greater decrease in O_3 relative to the same percent reduction in anthropogenic VOC. In contrast, the VOC-sensitive regime refers to situations in which a percent reduction in anthropogenic VOC

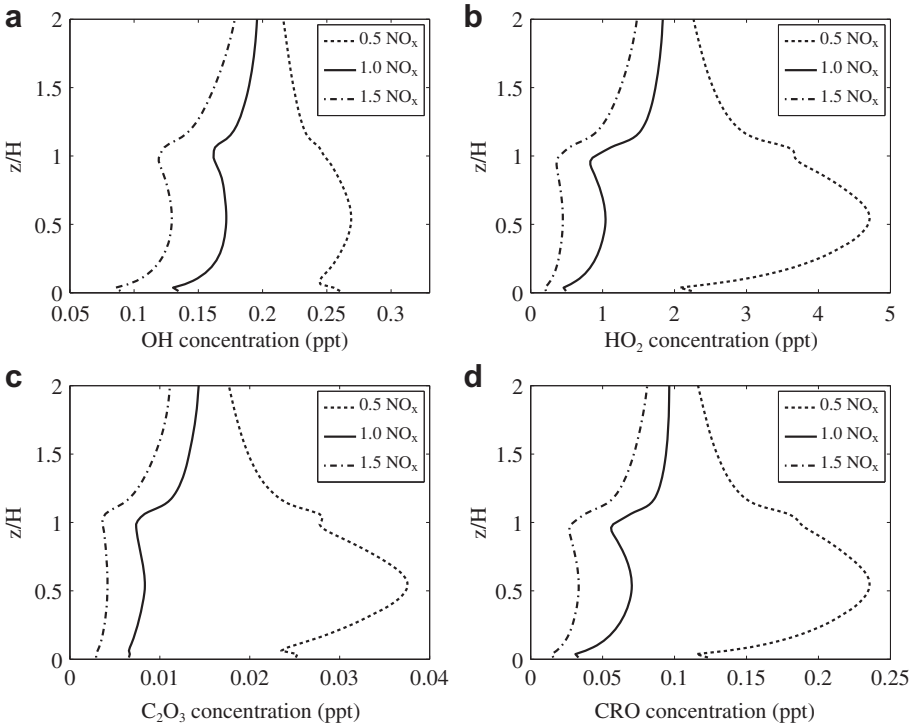

Fig. 9. Vertical profiles of the street canyon width-averaged concentrations of (a) OH, (b) HO_2, (c) C_2O_3, and (d) CRO for the emission scenarios of 0.5, 1.0, and 1.5 NO_x with 1.0 VOC.

results in a significantly greater decrease in O_3 relative to the same percent reduction in NO_x. The O_3–NO_x–VOC sensitivity has been widely studied for urban areas by comparing changes in O_3 concentration resulting from reductions in NO_x and VOC emissions. Previous studies found that the VOC-sensitive regime is general in megacities such as Paris (Deguillaume et al., 2008) and Mexico City (Lei et al., 2007; Song et al., 2010).

As analyzed above, however, the chemical characteristics in a street canyon are distinct from those in broad-scale urban areas because of the proximity of mobile sources. We evaluate

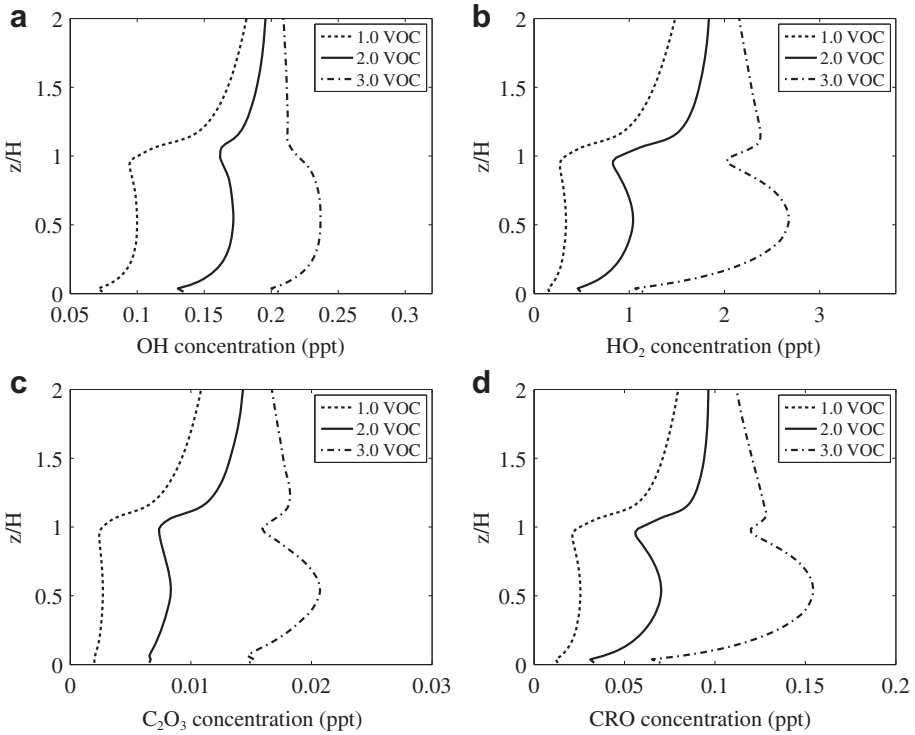

Fig. 10. Same as Fig. 9 but for the emission scenarios of 1.0, 2.0, and 3.0 VOC with 1.0 NO_x.

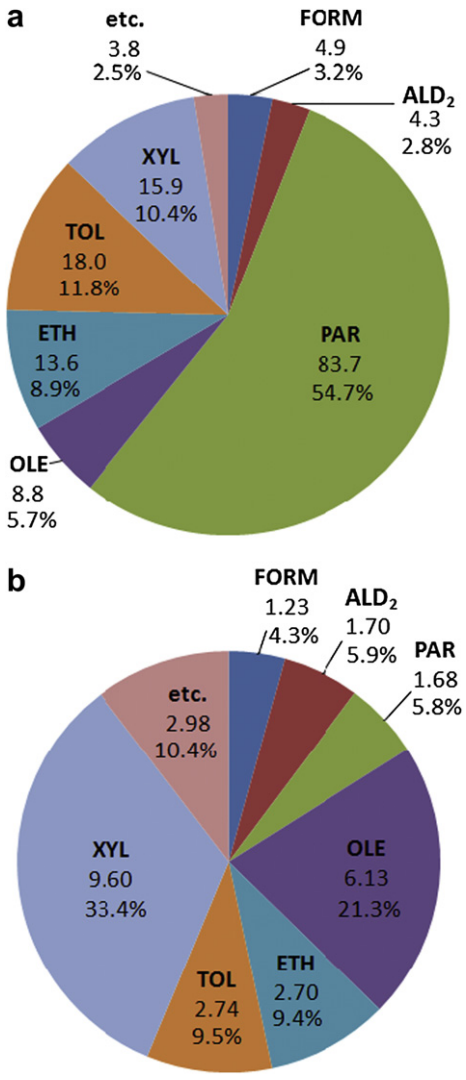

Fig. 11. Pie charts of the street canyon-averaged (a) concentrations (ppb) and (b) OH reactivities (s^{-1}) of VOCs for the emission scenario of 1.0 NO_x and 1.0 VOC.

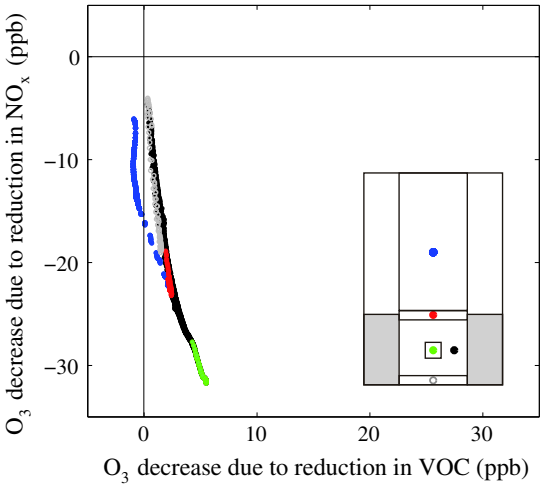

Fig. 12. Scatter diagram of decreases in O_3 concentration due to 50% reduction in NO_x (O_3 decrease due to NO_x) or VOC emission (O_3 decrease due to VOC). Note that negative values in O_3 decrease due to NO_x or VOC mean O_3 increases due to NO_x or VOC. Individual dots for each of the five different filled and open circles in the diagram correspond to grid points for each of the five different regions of the computational domain (inset).

O_3–NO_x–VOC sensitivity in the street canyon by comparing the O_3 concentrations of 3 emission scenarios (S1, S3, S11). The diagram of Sillman and West (2009) is used to identify chemical regimes. In the diagram, the location of each grid point in the numerical model is assigned to NO_x-sensitive, VOC-sensitive, mixed, NO_x titration, or no sensitivity regimes.

Following Sillman and West (2009), a scatter diagram of decreases in O_3 concentration due to reduction in NO_x emission level from 1.0 NO_x to 0.5 NO_x [O_3(S3) − O_3(S1) in the ordinate] and due to reduction in VOC emission level from 1.0 VOC to 0.5 VOC [O_3(S3) − O_3(S11) in the abscissa] is plotted in Fig. 12. Most locations in and above the street canyon belong to the NO_x titration regime based on the definition of Sillman and West (2009). They defined a location as dominated by the NO_x titration if the O_3 concentration increases by 5 ppb or more in response to reduced NO_x emission and does not decrease by 5 ppb or more in response to reduced VOC emission. In response to reduced NO_x emission level from 1.0 NO_x to 0.5 NO_x, increases in O_3 concentration are significant at all locations in and above the street canyon. These increases range from a few ppb near the street bottom to over 30 ppb near the center of the street canyon. In response to reduced VOC emission level from 1.0 VOC to 0.5 VOC, the locations near the street bottom rarely show changes in O_3 concentration. On the other hand, the locations near the center of the street canyon show comparable decreases in O_3 concentration due to the reduction in VOC emission level.

In the street canyon, where the NO-to-NO_2 ratio exceeds 1, the NO titration is a major sink of O_3 and more pronounced than the NO_2 photolysis. The street canyon-averaged chemical O_3 production is governed primarily by the O + O_2 reaction induced by the NO_2 photolysis. In contrast, the street canyon-averaged chemical O_3 loss is governed primarily by the NO titration and partly by the O_3 photolysis. Compared to the reactions, others are negligible. Although the effect of VOCs on the O_3 concentration is important through the radical chain, NO_x strongly affects O_3 not only by means of the radical chain but also by means of the NO titration. Consequently, the street canyon is a negatively NO_x-sensitive regime because of freshly emitted NO from mobile sources.

4. Summary

A CFD model that includes the CBM-IV was developed and used to investigate the dispersion of reactive species in and above a street canyon with a canyon aspect ratio of 1. A total of 14 emission scenarios of NO_x and VOC were analyzed. The model was validated against the field measurement data for NO_2 and NO_x concentrations, showing that the simulated concentrations are in good agreement with the measured concentrations. Three dispersion types were identified: NO-type, NO_2-type, and O_3-type dispersion that exhibit concentration maxima at the street bottom, near the center of the street canyon, and above the street canyon, respectively. For the base emission scenario, the number of reactive species is 9 in the NO-type dispersion, 10 in the NO_2-type dispersion, and 15 in the O_3-type dispersion. The dispersion type of any species except for the NO-type dispersion was shown to be dependent on the NO_x and VOC emission levels. As the NO_x emission level increases, the concentrations of species in the NO_2-type and O_3-type dispersion generally become more reduced in the street canyon than above it. In contrast, as the VOC emission level increases, the concentrations of species in the NO_2-type and O_3-type dispersion generally become more increased in the street canyon than above it. As a consequence of these concentration

changes in the street canyon, species in the O_3-type dispersion generally tends to be shifted to the NO_2-type dispersion when the VOC-to-NO_x emission ratio increases. It was found that the OH concentration increases as the VOC emission level increases but decreases as the NO_x emission level decreases, which means that the OH concentration tends to increase with the VOC-to-NO_x emission ratio. In this way, OH plays a key role in controlling the dispersion type of reactive species through the radical chain including HO_2, RO, and RO_2. Among the VOCs involved in this process, XYL and OLE are responsible for more than a half of the OH + RH reaction because of their high OH reactivities.

Because the NO-to-NO_2 ratio is high in the street canyon, the O_3 sensitivity to the NO_x and VOC emissions in the street canyon differs from that for broad-scale urban areas where the NO-to-NO_2 ratio is relatively low. The high NO-to-NO_2 ratio in the street canyon makes the NO titration of O_3 be more pronounced than the NO_2 photolysis. In the street canyon, the O_3 concentration is negatively correlated with the NO_x emission level but weakly correlated with the VOC emission level. Therefore, in contrast with the general finding that an urban area is generally a VOC-sensitive regime, the street canyon is a negatively NO_x-sensitive regime.

Acknowledgments

The authors are grateful to two anonymous reviewers for providing valuable comments that led to the improvements of the original manuscript. This work was supported by the National Research Foundation of Korea (NRF) grant funded by the Korea Ministry of Education, Science and Technology (MEST) (No. 2011-0017041) and also by the Brain Korea 21 Project (through the School of Earth and Environmental Sciences, Seoul National University).

References

Baik, J.-J., Kang, Y.-S., Kim, J.-J., 2007. Modeling reactive pollutant dispersion in an urban street canyon. Atmospheric Environment 41, 934–949.

Baker, J., Walker, H.L., Cai, X., 2004. A study of the dispersion and transport of reactive pollutants in and above street canyons – a large eddy simulation. Atmospheric Environment 38, 6883–6892.

Bossioli, E., Tombrou, M., Pilinis, C., 2002. Adapting the speciation of the VOCs emission inventory in the greater Athens area. Water, Air, and Soil Pollution: Focus 2, 141–153.

Carter, W.P.L., 1996. Condensed atmospheric photooxidation mechanisms for isoprene. Atmospheric Environment 30, 4275–4290.

Chan, T.L., Dong, G., Cheung, C.S., Leung, C.W., Wong, C.P., Hung, W.T., 2001. Monte Carlo simulation of nitrogen oxides dispersion from a vehicular exhaust plume and its sensitivity studies. Atmospheric Environment 35, 6117–6127.

Clements, A.L., Jia, Y., Denbleyker, A., McDonald-Buller, E., Fraser, M.P., Allen, D.T., Collins, D.R., Michel, E., Pudota, J., Sullivan, D., Zhu, Y., 2009. Air pollutant concentrations near three Texas roadways, part II: chemical characterization and transformation of pollutants. Atmospheric Environment 43, 4523–4534.

Deguillaume, L., Beekmann, M., Derognat, C., 2008. Uncertainty evaluation of ozone production and its sensitivity to emission changes over the Ile-de-France region during summer periods. Journal of Geophysical Research 113. doi:10.1029/2007JD009081.

Doraiswamy, P., Hogrefe, C., Hao, W., Henry, R.F., Civerolo, K., Ku, J.-Y., Sistla, G., Schwab, J.J., Demerjian, K.L., 2009. A diagnostic comparison of measured and model-predicted speciated VOC concentrations. Atmospheric Environment 43, 5759–5770.

Garmory, A., Kim, I.S., Britter, R.E., Mastorakos, E., 2009. Simulations of the dispersion of reactive pollutants in a street canyon, considering different chemical mechanisms and micromixing. Atmospheric Environment 43, 4670–4680.

Gery, M., Witten, G., Killus, J., Dodge, M., 1989. A photochemical kinetics mechanism for urban and regional scale computer modeling. Journal of Geophysical Research 94 (D10), 12925–12956.

Grawe, D., Cai, X.-M., Harrison, R.M., 2007. Large eddy simulation of shading effects on NO_2 and O_3 concentrations within an idealized street canyon. Atmospheric Environment 41, 7304–7314.

Hertel, O., Berkowicz, R., Christensen, J., 1993. Test of two numerical schemes for use in atmospheric transport-chemistry models. Atmospheric Environment 27A, 2591–2611.

Jacobson, M.Z., 2005. Fundamentals of Atmospheric Modeling, Cambridge, second ed., 813 pp.

Jenkin, M.E., Clemitshaw, K.C., 2000. Ozone and other secondary photochemical pollutants: chemical processes governing their formation in the planetary boundary layer. Atmospheric Envionment 34, 2499–2527.

Kang, Y.-S., Baik, J.-J., Kim, J.-J., 2008. Further studies of flow and reactive pollutant dispersion in a street canyon with bottom heating. Atmospheric Environment 42, 4964–4975.

Kim, D.-Y., Kim, J.-J., Oh, J.-H., Sen, P., 2008. A case study on emission management for reducing photochemical pollution over the Osaka bay area. Asia-Pacific Journal of Atmospheric Sciences 44 (4), 341–349.

Kim, J.-J., Baik, J.-J., 2004. A numerical study of the effects of ambient wind direction on flow and dispersion in urban street canyons using the RNG k–ε turbulence model. Atmospheric Environment 38, 3039–3048.

Lei, W., Foy, B., Zavala, M., Volkamer, R., Molina, L.T., 2007. Characterizing ozone production in the Mexico City metropolitan area: a case study using a chemical transport model. Atmospheric Chemistry and Physics 7, 1347–1366.

Liu, C.-H., Leung, D.Y.C., 2008. Numerical study on the ozone formation inside street canyons using a chemistry box model. Journal of Environmental Sciences 20, 832–837.

Martins, L.D., Andrade, M.F., 2008. Ozone formation potentials of volatile organic compounds and ozone sensitivity to their emission in the megacity of São Paulo, Brazil. Water, Air, and Soil Pollution 195, 201–213.

Peng, Y.P., Chen, K.S., Lai, C.H., Lu, P.J., Kao, J.H., 2006. Concentrations of H_2O_2 and HNO_3 and O_3–VOC–NO_x sensitivity in ambient air in southern Taiwan. Atmospheric Environment 40, 6741–6751.

Sillman, S., 1999. The relation between ozone, NO_x and hydrocarbons in urban and polluted rural environments. Atmospheric Environment 33, 1821–1845.

Sillman, S., West, J.J., 2009. Reactive nitrogen in Mexico City and its relation to ozone-precursor sensitivity: results from photochemical models. Atmospheric Chemistry and Physics 9, 3477–3489.

Smylie, M., Fieber, J.L., Myers, T.C., Burton, S., 1991. A preliminary examination of the impact on emissions and ozone air quality in Athens, Greece from various hypothetical motor vehicle control strategies. European Conference on New Fuels and Clean Air, 19 June 1991, Antwerp, Belgium.

Song, J., Lei, W., Bei, N., Zavala, M., Foy, B., Volkamer, R., Cardenas, B., Zheng, J., Zhang, R., Molina, L.T., 2010. Ozone response to emission changes: a modeling study during the MCMA-2006/MILAGRO campaign. Atmospheric Chemistry and Physics 10, 3827–3846.

Wang, Y.J., DenBleyker, A., McDonald-Buller, E., Allen, D., Zhang, K.M., 2011. Modeling the chemical evolution of nitrogen oxides near roadways. Atmospheric Environment 45, 43–52.

Zavala, M., Lei, W., Molina, M.J., Molina, L.T., 2009. Modeled and observed ozone sensitivity to mobile-source emissions in Mexico City. Atmospheric Chemistry and Physics 9, 39–55.

Zhu, Y., Pudota, J., Collins, D., Allen, D., Clements, A., DenBleyker, A., Fraser, M., Jia, Y., McDonald-Buller, E., Michel, E., 2009. Air pollutant concentrations near three Texas roadways, Part I: ultrafine particles. Atmospheric Environment 43, 4513–4522.